ELSEVIER

Chemical Engineering Journal 75 (1999) 105–111

Chemical Engineering Journal

www.elsevier.com/locate/cej

# Residence time distribution studies in a simulated tubular affinity membrane separator

Siamak Najarian*, B.J. Bellhouse

*Medical Engineering Unit, Department of Engineering Science, University of Oxford, 43 Banbury Road, Oxford OX2 6PE, UK*

Received 1 April 1996; received in revised form 31 March 1999; accepted 14 April 1999

**Abstract**

One of the key factors in designing an affinity membrane contactor is the flow pattern in the device. This paper presents a study carried out on the residence time distribution (RTD) of a tracer in a cross-flow tubular affinity module. For simplicity, no membrane was incorporated in the system. A tubular conduit with a total length of 0.7 m was designed and to improve the RTD of the tracer, various screw-threaded inserts were tested. The experimental tests for the RTDs in a channel with no inserts, a channel with a plain rod and a channel with helical inserts were performed and compared with the corresponding theoretical models. Two different methods of analyzing the data were adopted. The first method was based on the evaluation of the variance of the *E*-curves, and the second was based on the use of Fourier transform analysis. The experimental data showed that appropriate combination of pulsation frequency, piston stroke length, and geometry resulted in an optimum value for the Peclet number. This provides an explanation of why the capturing efficiency of the target species in membrane affinity separations is enhanced significantly by oscillatory flow. 

*Keywords:* Cross-flow; Affinity membrane; Residence time distribution; Peclet number; Oscillatory flow

## 1. Introduction

In membrane affinity separation processes, the build-up of solute/particles near the membrane–solution interface is one of the factors responsible for a reduction in performance at a given operating pressure [1]. Depending on the chemical and physical nature of the mixture, the effective film thickness for feed side mass transfer resistance can be reduced by increasing the solute diffusivity and decreasing the solvent viscosity. This film can also be diminished by promoting more efficient mixing in the vicinity of the membrane by means of thin channel design, mixing promoters, or simple stirring [2]. For flow through empty tubes, theories show that pulsing the flow might increase both heat and mass transfer from the wall to the fluid [3]. By applying pulsation in the case of laminar flow, the maximum velocity occurs not at the centerline but near the wall where high velocities are required to counteract concentration polarization [4].

At low Reynolds number, little or no mixing occurs in the radial direction and consequently important key factors such as, heat transfer, mass transfer and mixing within the contactors are relatively poor [5]. Radial mixing can be enhanced by operating in the turbulent flow regime. However, in the case of biological fluids, there is a high probability that turbulence damages the proteins and other shear sensitive constituents. To reduce this risk, it has been recommended by many workers to perform the process in the laminar regime [6–8]. It should be noted that even if the turbulent flow regime is chosen, the radial velocity components are typically one tenth of the axial velocity components, and still little improvement might be obtained [9]. To achieve a situation in which the vertical velocity is comparable to the horizontal velocity, the simultaneous application of flow deflectors (or mixing promoters) and flow pulsation may be beneficial.

Najarian et al. [10] have shown that by choosing a suitable combination of piston stroke length and pulsation frequency, it was possible to enhance the capturing efficiency of the target molecules on the binding sites of a modified microfiltration affinity membrane. In their studies, bovine serum albumin acted as the target molecule and a textile dye (Cibacron Blue F3G-A) as the ligand. The major concern

*Present address. Biomedical Engineering Department, Amirkabir University of Technology, Postcode 15914, Tehran, Iran. Tel.: +98-21-649-5655; fax: +98-21-641-2437

*E-mail address*: najarian@cic.aku.ac.ir (S. Najarian)

1385-8947/99/$ – see front matter 
PII: S1385-8947(99)00091-1

of this research is to get a better understanding regarding the above phenomena. It was suggested that the flow pattern in the tubular channel used for the process could have had an impact on the behaviour of the system. Due to the low rate of mass transfer in the radial direction (for steady laminar flow regime), the performance of any contacting devices reduces dramatically. As a result of this, when it is intended to separate a particular reactant from the fluid-phase, the chance of being captured by the immobilized ligand will not be the same for all of the reactant molecules [11]. This could mean that the outlet of the reactor ( i.e., retentate side) should be recycled to give another chance to the unreacted molecules. The more the amount of unreacted species (i.e., low reaction conversion), the more it will take to process a certain amount of reacting mixture. Ideally, the most efficient contacting patterns are those which require fewer passes through the reactor at similar operational conditions.

In our setup, the radial velocity component can be increased and, therefore, more mixing will occur in the radial direction. However, because the turbulent flow regime should be avoided, another alternative is the use of oscillatory flow in the laminar regime [12].

## 2. Materials and methods

### 2.1. Tubular conduit

A tubular conduit with the specifications shown in Fig. 1 was designed and used for the stimulus-response experiments. In this figure, the minimum channel gap ($2h$) is (12.42–11.92)/2 = 0.25 mm. All the major components were constructed with perspex (polymethylmethacrylate). The pistons were made of stainless-steel and the total length of the device was 0.7 m. The screw-threaded (or helical) inserts were made of moulded epoxy resin (3.5 and 5.5 mm pitch) and were centralized in the tubular channel by means

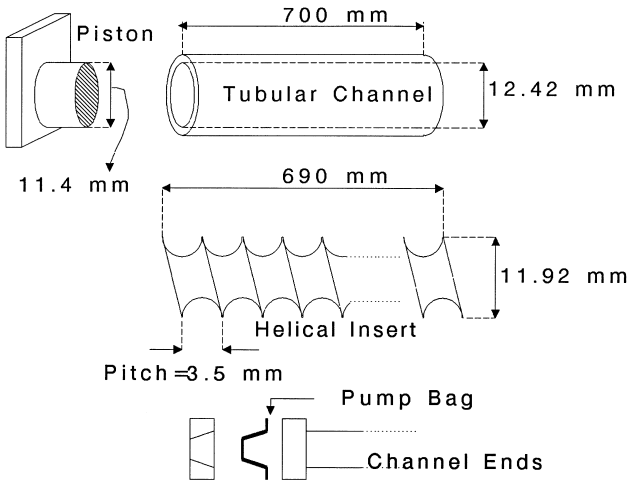


Fig. 1. Schematic representation of the tubular conduit used in the RTD experiments.

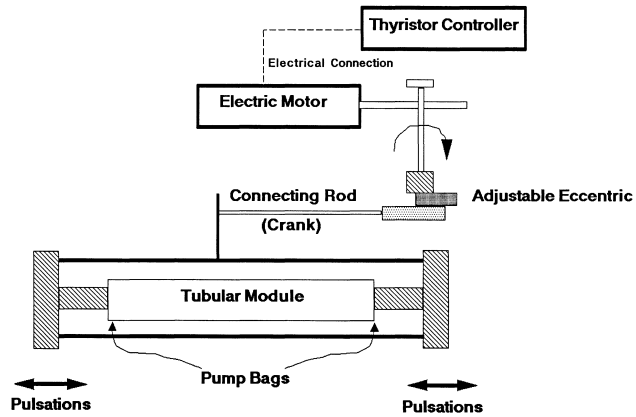


Fig. 2. Sketch showing the pulsed flow generator.

of a recess. Apart from the helical inserts, various plain rods (smooth surface finish) with different outside diameters were also tested. For simplicity, no membrane was employed in these runs, and the walls of the conduit were essentially impermeable.

### 2.2. Oscillatory flow generator

A Scotch yoke device was used to generate oscillatory flow. This device contained four separate components and its schematic representation is shown in Fig. 2. The first component was an electric motor (Parvalux, Electric Motors Ltd., UK) the rotational speed of which could be varied through the use of the second component, a thyristor controller for d.c. shunt motors (BSL 025, Electron). A crank (the third component), driven by the motor was used to produce horizontal oscillations of the pistons (the fourth component) mounted at each end of the conduit. The frequency of oscillation was readily controlled by varying the speed of the motor, resulting in a frequency range of 0–5 Hz, whilst the stroke length of oscillation was changed separately in the range of 0–8 mm. To calibrate the thyristor controller, an optical tachometer (TM-2011, RS Components Ltd.) was utilized. The backward and forward movement of the stainless-steel pistons actuated the polyurethane pump bags. Each cylindrical piston had a diameter of 11.4 mm which produced a piston area of 1.03 $cm^2$. All tubing used in these sets of experiments were made of silicone rubber or polyvinyl chloride.

### 2.3. RTD test rig

Fresh distilled water served as the process fluid, and was fed to the tubular conduit using a roller pump (Watson-Marlow 501U). In all runs, the device was positioned horizontally. The outlet stream of the tubular device was diverted to a recording spectrophotometer (UV-160, Shimadzu), where the optical density of the tracer injected was measured and stored for further analysis. The injection of tracer took place at the inlet of the conduit via a 3-way valve

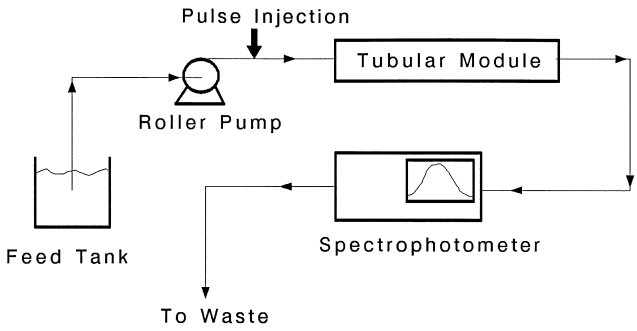


Fig. 3. Schematic diagram showing the circuit used for RTD measurements in tubular rig.

incorporated into the inlet port. The detailed sketch of this operation is illustrated in Fig. 3. The outlet stream of the spectrophotometer flowed into a waste reservoir.

The volume of the flow circuit employed was held to a minimum. This made the time that fluid spent in the outlet line, before it left the spectrophotometer, very small compared to the residence time in the channel. A constant temperature bath was used to maintain the temperature of the working fluid at 20°C.

### 2.4. Tracer specifications

Methylene blue (Aldrich; 31,911-2) was employed as the tracer. To inject this substance into the system, a repetitive pipette (Eppendorf Pipettemen) was used. Each time a constant volume of 0.5 ml (0.05 wt.% solution in water) of methylene blue was injected through a 3-way valve. Another method of injection was also carried out by simply using a syringe. Unlike the repetitive pipette, the results obtained by syringe injection were not very repeatable. Therefore, the former method was adopted throughout this set of runs. The optical density of the tracer at the outlet stream was detected at a wavelength of 663 nm. Since a linear relationship was found between the optical density and the concentration of the tracer, mathematical analysis was undertaken directly on the output data of the spectrophotometer.

### 2.5. Characterization of an RTD curve

For a $C$ versus $t$ curve, the mean is defined as [13,14]:

$$t_m = \frac{\int_0^\infty tC\mathrm{d}t}{\int_0^\infty C\mathrm{d}t} \tag{1}$$

and the definition of variance as:

$$\sigma_t^2 = \frac{\int_0^\infty (t-t_m)^2 C\mathrm{d}t}{\int_0^\infty C\mathrm{d}t} \tag{2}$$

Due to the simplicity of working with dimensionless groups, it was more appropriate to use the following definitions [15–17]:

$$E_t = \frac{C}{\int_0^\infty C\mathrm{d}t} \tag{3}$$

$$\theta = \frac{t}{t_m} \tag{4}$$

$$\sigma_\theta^2 = \frac{\sigma_t^2}{t_m^2} = \int_0^\infty \left(\frac{t}{t_m}\right)^2 E_t\mathrm{d}t - 1 \tag{5}$$

The probability density function $E$ was chosen so that the area beneath the curve equalled unity, also $E_\theta = t_m E_t$. The quantity $\sigma_\theta^2$ is a dimensionless variance and can be related to the Peclet number by the following equation [13]:

$$Pe = \frac{8}{\sqrt{8\sigma_\theta^2 + 1} - 1} \tag{6}$$

A sharp spike at $\theta = 1$ means that the flow pattern in the channel approaches plug flow. It also suggests that the axial dispersion, which reduces the capturing efficiency, has been decreased.

During the experimental tests, it was noticed that in some cases (such as the insertless channel) the tailing of the curves was so long that the measurement of the variance was badly influenced by the baseline noise encountered in the spectrophotometric measurement. Therefore, it was difficult to judge at which point the data should be truncated. This is the reason why another method of analysis was also utilized, which was based on frequency response of the system.

The aim of these calculations is to compare $y_O(t)$, the observed response with $y_P(t)$, the predicted response. For complicated physical phenomena, such as RTD, it may be very difficult to find and compute the predicted response. This happens because of the mathematical complexity involves in solving the governing partial differential equations (PDEs) describing the dispersion process. To eliminate this difficulty, the variable $s$ in the Laplace domain was changed to $j\omega$ in the frequency domain and, therefore, $Y_P(j\omega)$ was obtained instead of $y_P(t)$. Thus, the comparison was made between $Y_P(j\omega)$ and $Y_O(j\omega)$. To obtain $Y_O(j\omega)$, the experimental $E$-curves were transferred to the frequency domain, through the use of Fourier transforms. Finally, by the variation of $Pe$, the matching between $Y_P(j\omega)$ and $Y_O(j\omega)$ was performed.

The Fourier transform of the experimental data can be calculated via the following equations [18]:

$$Y_O(j\omega) = \int_0^\infty y_O(t)\mathrm{e}^{-\mathrm{j}\omega t}\,\mathrm{d}t \tag{7}$$

or

$$Y_O(j\omega) = \int_0^\infty y(t)\cos(\omega t)\mathrm{d}t - j\int_0^\infty y_O(t)\sin(\omega t)\mathrm{d}t \tag{8}$$

or in a more consolidated form,

$$Y_O(j\omega) = R(\omega) + j(\omega) \tag{9}$$

where $j = (-1)^{1/2}$. The theoretical data in the frequency domain were extracted from the following model [19]:

$$Y_P(j\omega) = (1+\alpha^2)^{-1/4} e^{((Pe/2)-(Pe/2)(1+\alpha^2)^{0.25}\cos\beta)} \tag{10}$$

where $\alpha$ and $\beta$ are defined as follows:

$$\alpha = \frac{4\omega t_m}{Pe} \tag{11}$$

$$\beta = \tfrac{1}{2}\arctan(\alpha) \tag{12}$$

## 3. Experimental results

### 3.1. RTD in an insertless tubular conduit

To begin with, it was decided not to place any insert in the tubular conduit and to investigate how effective was the role of oscillatory flow in changing the velocity profile of the tracer molecules. The inlet flow rate was set at 68 ml/min and due to the transparency of the device, it was possible to detect the flow pattern visually. Apart from the results of theoretical analysis, the retention of the dye molecules was quite evident on the walls. This was a clear indication that the rate of radial mixing was very small. Experimental data shown in Fig. 4 denote a sharp increase of concentration followed by a long tail, typical of this type of operation.

Various combinations of piston stroke length (i.e., $k$ = 1–9 mm) and frequency (i.e., $f$ = 1–6 Hz) had little effect on the shape of the $E$-curves. The theoretical models described earlier cannot be applied confidently to these data. This is because when the effect of molecular diffusion in the radial direction is small, the axial dispersion model is no longer valid. If all the molecular diffusion can be ignored, the following theoretical equation is applicable [19]:

$$E_\theta = \begin{bmatrix} 0, & \text{for } \theta<0.5 \\ 12\theta^3, & \text{for } \theta<0.5 \end{bmatrix} \tag{13}$$

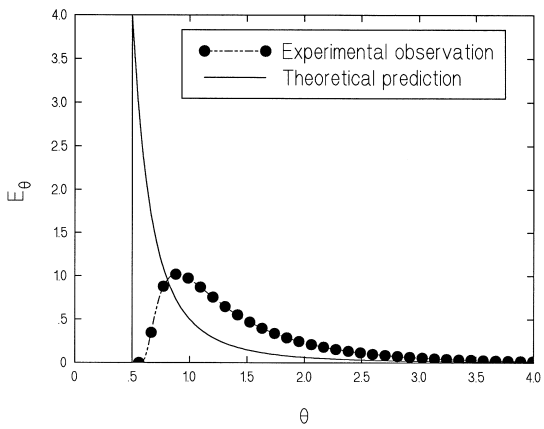


Fig. 4. RTD observed in the insertless tubular conduit.

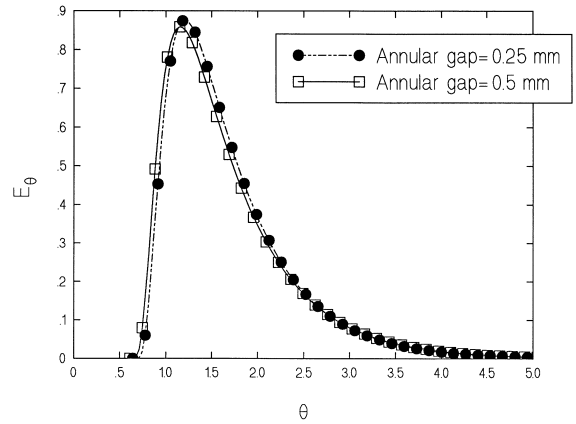


Fig. 5. RTD observed in the tubular conduit equipped with two different types of plain rod inserts.

For comparison, the above equation is also plotted in Fig. 4. Although the critical $\theta$ at which the first tracer molecule emerges at the outlet is quite similar in both curves (i.e., $\theta_{C,exp} = 0.53$ and $\theta_{C,theo} = 0.5$), the general shape is not. This could be attributed to the fact that the pattern observed is an intermediate case between the two extreme cases of high and low contribution of molecular diffusion.

### 3.2. RTD in annuli

Two plain rods were placed, in turn, in the tubular conduit and similar experiments were carried out. The annular gaps studied were 0.25 and 0.5 mm. All the operating conditions were the same as those used in the insertless tubular conduit. The experimental curves are presented in Fig. 5. As can be seen from this figure, the general trend of the observed RTDs is quite similar to each other. However, an annular gap of 0.25 mm resulted in a marginally narrower distribution with the critical $\theta$ shifting towards the right hand side. Both systems led to relatively long tailing of the distribution curves which practically coincided at $\theta \approx 2.5$. Theoretical studies performed by Nigam et al. [19] predict a value of $\theta_C = 0.66$. This differs from the range of 0.58–0.61 obtained here. However, the experimental work carried out by Nigam et al. did not verify their theoretical findings, and consistently underestimated the $\theta_{C,theo}$. It was found that the RTD curves for the annuli were all insensitive to flow pulsation.

### 3.3. RTD in the tubular conduit equipped with helical inserts (2h = 0)

Various geometries of helical inserts were tested, and to investigate the influence of leakage flow through the annular gap, a set of runs was carried out with no annular gap (i.e., $2h = 0$). In other words, the insert was in close contact with the outer casing. Fig. 6 illustrates the residence time distribution curve for the no-gap set-up ($Re_n = 4$, $Re_o$ = 5–35).

At this stage, it is of great importance to make a comparison between the variance of the $E_\theta$-curves in Fig. 6 with those of the annular geometries. It must be noted that the

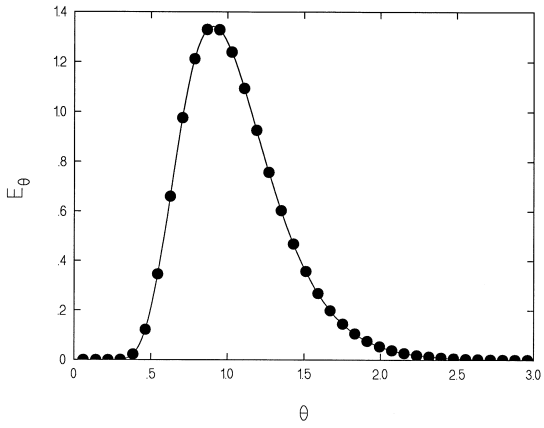


Fig. 6. RTD observed in the tubular conduit equipped with helical inserts ($2h = 0$).

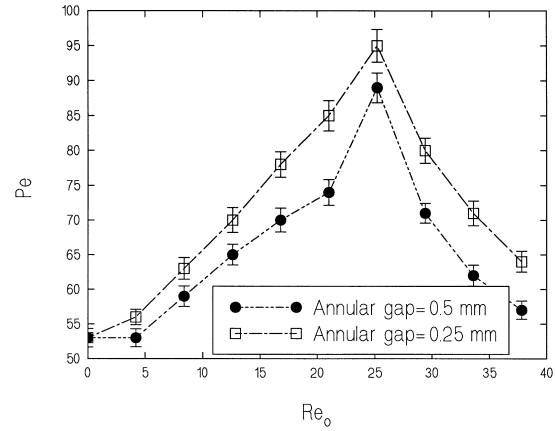


Fig. 7. Variation of *Pe* with $Re_o$ (or pulsation frequency) for $k = 4$ mm, $St = 9\times10^{-4}$ and $Re_n = 4$. Number of runs for each data point = 6.

reduction of axial dispersion coefficient can be inferred from the rise in the value of the Peclet number. Table 1 summarizes these findings. It appears that the spiral path of the insert improved the age distribution of the molecules, a fact which is signified by a rise in the Peclet number. Again, oscillations did not change the RTD curve.

### 3.4. RTD in the tubular conduit equipped with helical inserts (2h # 0)

Placement of an insert in the tubular device was always accompanied by a sharpening in the residence time distribution curves and the disappearance of tailing. In this part of the investigation, similar experimental work was carried out, but with a gap between the insert and the casing. Unlike the other cases mentioned previously, these distributions were changed significantly by flow pulsation. the dimensionless parameters used in this study are defined as follows [20–24]:

$$Re_n = \frac{Q_n}{2\pi d_m \nu} \tag{14}$$

$$Re_o = \frac{fkA_P}{2d_m\nu} \tag{15}$$

$$St = \frac{2h^2 d_m}{kA_P} \tag{16}$$

where $Re_n$ is the net Reynolds number, $Re_o$ is the oscillatory Reynolds number and *St* is the Strouhal number. Fig. 7 shows the variation of the Peclet number with the frequency of pulsation. For both $2h = 0.25$ and 0.5 mm, the Peclet number reaches a maximum at an oscillatory Reynolds number of 25, corresponding to a frequency of 6 Hz and a fixed stroke length of $k = 4$ mm. As the frequency is varied from 0 to 6 Hz, the effect of pulsatile flow is such that the axial dispersion is decreased as the flow pattern approaches plug flow. Beyond this limit, the property of plug flow is reduced and pulsation adversely affects the RTD curves. Although a similar trend was observed when piston stroke length was varied, the difference between the performance of the two helix pitches was negligible. These data are presented in Fig. 8. Up to a piston stroke length of 4 mm, pulsation improves the RTD of the tracer, whilst above this critical value, axial dispersion rises again.

Table 1
Comparison between two types of plain rod inserts ($2h = 0.25$ and 0.5 mm) with the helical inserts

| Type of insert | $r_\theta^2$ | *Pe* |
|---|---|---|
| Plain rod ($2h$ = 0.5 mm) | 0.516 | 6.3 |
| Plain rod ($2h$ = 0.25 mm) | 0.478 | 6.6 |
| Helical insert (pitch = 3.5 mm, $2h = 0$) | 0.109 | 21.7 |
| Helical insert (pitch = 3.5 mm, $2h = 0.25$ mm, steady flow) | 0.040 | 53.0 |

### 3.5. Comparison between theoretical prediction and experimental data

A frequency response method based on Fourier transform analysis proved to be a suitable mathematical tool for

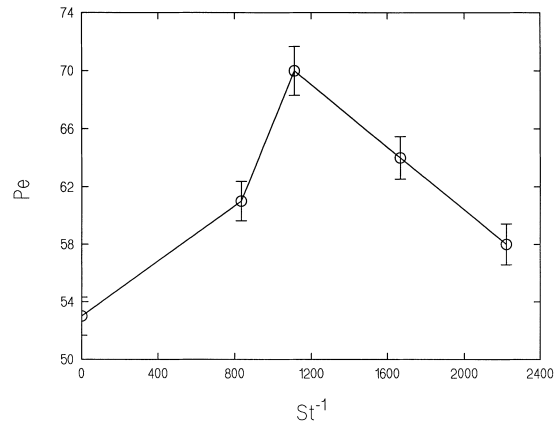


Fig. 8. Effect of $St^{-1}$ on Peclet number. Number of runs for each data point = 8.

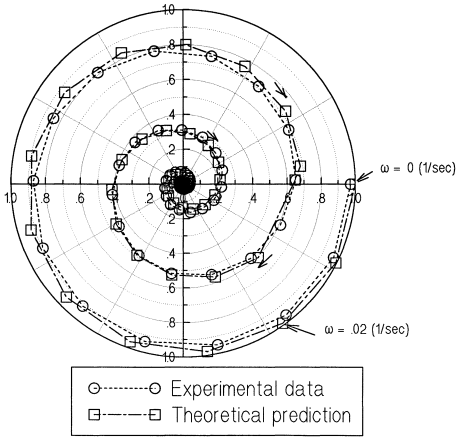


Fig. 9. Polar plot showing the comparison between the theoretical prediction and the experimental data.

analyzing the RTD studies. One of the features of this approach was the possibility of the use of a polar plot for visual detection of the matching property of the model. By using a Peclet number of 95 (for $t_m = 0.77$ min), good agreement was observed between the theoretical prediction and the experimental data ($f = 4$ Hz and $k = 4$ mm). The polar plot showing this characteristic is presented in Fig. 9. Each point in this figure corresponds to a unique angular frequency of $\omega$. As $\omega$ increases from zero to infinity, the spiral path of the points moves closer towards the centre of the polar plot.

## 4. Conclusions

The main motivation for the work reported in this paper was the findings of our previous investigation regarding the beneficial influence of oscillatory flow on the interaction between bovine serum albumin and a dye-ligand affinity membrane. The geometry of the module was tubular and the mode of operation was cross-flow. To investigate the above observations, a tubular conduit similar to the one used in the affinity tests was designed and the response of the injection of a tracer was analyzed using mathematical methods in RTD studies. Three broad groups of channel internal configuration were covered. The first group was the open tube (insertless) system. It was noticed that due to the parabolic velocity of the flow front, there was a wide range of age distribution for the tracer molecules appearing at the outlet of the system. By comparing the experimental curve with the theoretical one, it was found that although the critical $\theta$ at which the first tracer molecules emerged at the outlet was similar ($\theta_{C,exp} = 0.53$ and $\theta_{C,theo} = 0.5$), the general shape was not. The second group was concerned with flow in an annular gap between two concentric cylindrical tubes. Bare perspex rods were used as inserts to simulate this geometry. The general behaviour of the RTD curves in the first two configurations was similar, although a slight delay in the critical value of $\theta$ was noticed in the annuli. In the third configuration, helical inserts were employed as the mixing promoters. The Peclet number obtained for a helical insert with no gap ($2h = 0$) was 21.7, which was a factor of 3.2 higher than that for a plain rod with $2h = 0.25$ mm. Comparison between two helix pitches (3.5 and 5.5 mm) showed only a marginal improvement in RTD, when 3.5 mm pitch was utilized. In terms of both frequency and piston stroke length, there was an optimum value which could maximize the value of the Peclet number.

To analyze the experimental observations, two different mathematical methods were adopted. The first method was based on the calculation of mean residence time together with the variance of the observed RTD curve. These parameters were then related to *Pe*, which is an indication of axial dispersion in the reactor. Due to the relatively low values of variance obtained from the experimental data, the choice of Eq. (10) for mathematical modelling of the process was rather arbitrary. The assumption used in this model was based on the open vessel boundary conditions. Another approach applied to the experimental data was based on the frequency domain analysis of the stimulus-response runs and good agreement was observed between the two mathematical approaches.

## 5. Nomenclature

| | |
|---|---|
| $A_P$ | piston cross-sectional area ($m^2$) |
| $C$ | tracer concentration |
| $D$ | axial dispersion coefficient ($m^2/s$) |
| $d_m$ | mean diameter (m) |
| $E_q$ | dimensionless age distribution function |
| $E_t$ | dimensional age distribution function ($s^{-1}$) |
| $f$ | pulsation frequency (Hz) |
| $h$ | half of the minimum channel gap (m) |
| $I(\omega)$ | imaginary part of Fourier transform function |
| j | $(-1)^{1/2}$ |
| $k$ | piston stroke length (m) |
| $L$ | channel length (m) |
| $Pe$ | Peclet number, $(u_n L)/D$ |
| $Q_n$ | net volumetric flow rate ($m^3/s$) |
| $R(\omega)$ | real part of Fourier transform function |
| $Re_n$ | net Reynolds number, $Q_n/(2pd_m n)$ |
| $Re_o$ | oscillatory Reynolds number, $(fkA_P)/(2d_m n)$ |
| $s$ | Laplace transform variable |
| $St$ | Strouhal number, $(2h^2 d_m)/(kA_P)$ |
| $t$ | dimensionless time (s) |
| $t_m$ | mean residence time (s) |
| $u_n$ | net fluid velocity (m/s) |
| $y_O(t)$ | observed response function in time domain |
| $y_P(t)$ | predicted response function in time domain |
| $Y_O(t)$ | observed response function in frequency domain |
| $Y_P(j\omega)$ | predicted response function in frequency domain |

### 5.1. Greek letters

| | |
|---|---|
| $\alpha$ | $(4\omega t_m)/Pe$ |
| $\beta$ | 0.5 arctan ($\alpha$) |
| $\theta$ | dimensionless residence time, $t/t_m$ |
| $\theta_{C,exp}$ | experimental critical $\theta$ |
| $\theta_{C,theo}$ | theoretical critical $\theta$ |
| $\nu$ | kinematic viscosity ($m^2/s$) |
| $\sigma_\theta^2$ | dimensionless variance |
| $\sigma_t^2$ | dimensional variance ($s^2$) |
| $\omega$ | angular frequency ($s^{-1}$) |

### 5.2. Subscripts

| | |
|---|---|
| C | critical |
| m | mean |
| n | net |
| O | observed; oscillatory |
| P | predicted; piston |
| $t$ | dimensional time |
| $\theta$ | dimensionless time |

### 5.3. Abbreviations

| | |
|---|---|
| PDE | partial differential equation |
| RTD | residence time distribution |

## Acknowledgements

The financial support of the Southern Trust is gratefully acknowledged.

## References

[1] M. Unarska, P.A. Davies, M.P. Esnouf, B.J. Bellhouse, J. Chromatogr. 519 (1990) 53–67.
[2] S. Najarian, B.J. Bellhouse, J. Membr. Sci. 112 (1996).
[3] H. Schlichting, Boundary-Layer Theory, McGraw-Hill, 7th ed., 1968.
[4] M.R. Mackley, The Chem. Engineer, Feb. (1987) 18–20.
[5] M.R. Mackley, X. Ni, Chem. Eng. Sci. 46 (1991) 3139–3151.
[6] J.W. Stairmand, B.J. Bellhouse, Z. Jamal, R.W.H. Lewis, J.R. Urban, C.C. Entwistle, Life Supports Systems 4 (1986) 193–204.
[7] B.J. Bellhouse, I.J. Sobey, S. Alani, B.M. DeBlois, Bioseparation 4 (1994) 127–138.
[8] B.J. Bellhouse, R.W.H. Lewis, Trans. Am. Soc. Artif. Int. Organs 34 (1988) 747–754.
[9] M.E. Mackay, M.R. Mackley, Y. Wang, Trans. IChem E 69 (1991) 506–513.
[10] S. Najarian, B.J. Bellhouse, J. Biotechnol. Progress 13 (1997) 113.
[11] S. Najarian, D.Phil. Thesis, University of Oxford, 1995.
[12] I.J. Sobey, J. Fluid Mech. 151 (1985) 395–426.
[13] H.S. Fogler, Elements of Chemical Reaction Engineering, 2nd ed., Prentice-Hall, 1992.
[14] A.W. Dickens, M.R. Mackley, H.R. Williams, Chem. Eng. Sci. 44 (1989) 1471–1479.
[15] P.I. Pudjiono, N.S. Tavare, J. Garside, K.D.P. Nigam, Chem. Eng. J. 48 (1992) 101–110.
[16] L.G. Gibilara, Chem. Eng. Sci. 33 (1978) 487–492.
[17] W.C. Clements, Chem. Eng. Sci. 24 (1969) 957–963.
[18] J.R. Hays, W.C. Clements, T.R. Harris, AIChE J. March (1967) 374–378.
[19] K.D.P. Nigam, K. Vasudeva, Ind. Eng. Chem. Process Des. Dev. 15 (1976) 473–476.
[20] S. Najarian, B.J. Bellhouse, J. Membr. Sci. 114 (1996).
[21] T. Nishimura, A. Tarumoto, Y. Kawamura, Int. J. Heat Mass Transfer 30 (1987) 1007–1015.
[22] T. Nishimura, H. Miyashita, S. Murakami, Y. Kawamura, J. Chem. Eng. Japan 22 (1989) 505–511.
[23] S. Najarian, B.J. Bellhouse, Proceedings of the 36th Rocky Mountain Bioengineering Symposium, Colorado, USA, 1999.
[24] B.J. Bellhouse, M.P. Esnouf, Bin Gao, S. Najarian, J.S. Henderson, Proceedings of the 5th World Congress of Chemical Engineering & Artificial Organs, San Diego, USA, 1996.